the plant journal

SEB Society for Experimental Biology

The Plant Journal (2013) **73,** 617–627 doi: 10.1111/tpj.12061

The pollen tube: a soft shell with a hard core

Hannes Vogler[1], Christian Draeger[1], Alain Weber[2], Dimitris Felekis[3], Christof Eichenberger[1], Anne-Lise Routier-Kierzkowska[2], Aurélien Boisson-Dernier[1], Christoph Ringli[1], Bradley J. Nelson[3,*], Richard S. Smith[2,*] and Ueli Grossniklaus[1,*]

[1]*Institute of Plant Biology and Zürich-Basel Plant Science Center, University of Zürich, Zollikerstrasse 107, CH 8008, Zürich,*

[2]*Institute of Plant Sciences, University of Bern, Altenbergrain 21, CH 3013 Bern, and*

[3]*Institute of Robotics and Intelligent Systems, ETHZ, Tannenstrasse 3, CH 8092 Zürich, Switzerland*

Received 23 May 2012; revised 23 October 2012; accepted 25 October 2012; published online 10 December 2012.
*For correspondence (e-mails bnelson@ethz.ch; Richard.Smith@ips.unibe.ch; grossnik@botinst.uzh.ch).

SUMMARY

Plant cell expansion is controlled by a fine-tuned balance between intracellular turgor pressure, cell wall loosening and cell wall biosynthesis. To understand these processes, it is important to gain in-depth knowledge of cell wall mechanics. Pollen tubes are tip-growing cells that provide an ideal system to study mechanical properties at the single cell level. With the available approaches it was not easy to measure important mechanical parameters of pollen tubes, such as the elasticity of the cell wall. We used a cellular force microscope (CFM) to measure the apparent stiffness of lily pollen tubes. In combination with a mechanical model based on the finite element method (FEM), this allowed us to calculate turgor pressure and cell wall elasticity, which we found to be around 0.3 MPa and 20–90 MPa, respectively. Furthermore, and in contrast to previous reports, we showed that the difference in stiffness between the pollen tube tip and the shank can be explained solely by the geometry of the pollen tube. CFM, in combination with an FEM-based model, provides a powerful method to evaluate important mechanical parameters of single, growing cells. Our findings indicate that the cell wall of growing pollen tubes has mechanical properties similar to rubber. This suggests that a fully turgid pollen tube is a relatively stiff, yet flexible cell that can react very quickly to obstacles or attractants by adjusting the direction of growth on its way through the female transmitting tissue.

Keywords: pollen tube, cell wall, turgor pressure, Young's modulus, cellular force microscope, finite element method.

INTRODUCTION

The mechanical properties of cells and tissues have become an important aspect in understanding biological processes. During morphogenesis, mechanical stimuli were recently shown to be involved in the induction of embryonic development (Fernandez-Sanchez *et al.*, 2010), and in the control of growth processes in both animals and plants (Martin, 2010; Mirabet *et al.*, 2011).

Here, we study the mechanical properties of pollen tubes, which are extremely fast-growing cells that cover large distances to deliver the male gametes to the female gametophytes in the ovary of flowering plants. As growth is restricted to the tube tip, the cell wall in this area must be deformable, and is subject to a highly dynamic integration of new cell wall and membrane material, whereas in the distal part (shank), the wall is more static to resist turgor pressure. Indeed, it was shown that the composition of the pollen tube cell wall is different in the tip and in the shank. Typically, the tip of angiosperm pollen tubes consists of a single layer of highly methyl-esterified pectins. At 5–10 μm behind the tip, low quantities of cellulose are incorporated into the cell wall and pectins are de-esterified. A second layer, mainly containing callose, is deposited 20–30 μm behind the tip (Mascarenhas, 1975). A lot is known about the molecular regulation of pollen tube growth (reviewed in Qin and Yang, 2011; Hepler *et al.*, 2012), but only recently the instrumentation to study the mechanical aspects of cell expansion *in vivo* has become available (Geitmann and Parre, 2004; Parre and Geitmann, 2005; Zerzour *et al.*, 2009).

Turgor pressure is a relevant driving force of plant cell expansion, a process that is limited by the capability of the cell wall to extend. The plant cell wall is a complex composite material composed of cellulose microfibrils that are connected by a hemicellulose network and embedded in a pectin matrix containing structural proteins (reviewed in Cosgrove, 2005; Burton *et al.*, 2010). Precise control of the

internal pressure and stress relaxation in the cell wall allows for cell expansion.

From a mechanical point of view, the cell wall is under tensile stress mainly created by turgor pressure (Wei and Lintilhac, 2007). Because growth depends largely on the in-plane extension of the cell wall, it is important to directly measure in-plane elasticity. Several methods have been described to measure the Young's modulus, which is a measure of the stiffness of a linear elastic material (Young, 1845; Geitmann, 2006). Tensile tests have been applied to isolated cell wall compounds, intact isolated cell walls or entire pieces of tissue using extensiometers (Cosgrove, 1993; Kutschera, 1996; Chanliaud and Gidley, 1999; Edge *et al.*, 2000; Wei *et al.*, 2006). However, experiments on single, living cells are rare, mainly because it is difficult to isolate individual cells from tissues without damaging the cell wall. Furthermore, tensile tests have the disadvantage that it is not possible to measure local differences in the mechanical properties of the cell walls of individual cells.

The pressure probe is the only device that allows the direct measurement of turgor pressure. It has also been used to measure fluxes across the plasma membrane and elastic properties of single cells by applying changes in turgor pressure (reviewed in Tomos and Leigh, 1999; Pertl *et al.*, 2010). However, the method is invasive and does not allow the experimentalist to make several measurements in different areas of the same cell. As a consequence, as in the case of tensile tests, it is not possible to find local differences in the mechanical properties of the cell wall.

Nano- or micro-indentation approaches determine cellular stiffness by causing minute, local deformations of the cell and measuring the resulting forces. Atomic force microscopy (AFM) has proven to be instrumental for measuring the local elastic properties of single cells like fungal hyphae (Zhao *et al.*, 2005), as well as of entire tissues, such as the shoot apical meristem (Milani *et al.*, 2011; Peaucelle *et al.*, 2011). Similar in concept but using larger probes, micro-indentation techniques have been used to assess the mechanical properties of pollen tubes (Geitmann and Parre, 2004). Both methods do not damage the cell, and are therefore suitable to measure the stiffness of single cells or tissues. Whereas AFM offers a high degree of automation and resolution, it has a limited scanning area and the applied forces are too small to sufficiently indent the wall of fully turgid cells. Hence, the cell wall is compressed on a tiny surface rather than stretched, such that only conclusions about the elasticity perpendicular to, but not parallel with, the surface can be drawn. The larger micro-indentation device provides more flexibility in the scanning range and is capable of measuring in-plane elasticity, but lacks automation and is not commercially available. In all of these indentation methods the stiffness measured does not only reflect the mechanical properties of the cell wall. Additional parameters that contribute to the cellular stiffness are turgor pressure (Smith *et al.*, 1998; Wang *et al.*, 2004), as well as cell and indenter geometry (Bolduc *et al.*, 2006). Therefore, the stiffness values obtained are referred to as 'apparent stiffness' (Zamir and Taber, 2004).

Despite the large amount of work that has been invested into the determination of the mechanical properties of pollen tubes, there are still considerable gaps in our knowledge. The values for turgor pressure vary by a factor of three or more, depending on the method of measurement (Benkert *et al.*, 1997). No values at all are available for the Young's modulus, a measure of elastic properties, of the pollen tube cell wall. Here we use a cellular force microscope (CFM), a flexible microrobotic system, in combination with osmotic treatments, to measure the mechanical properties of living and growing pollen tubes in a non-invasive manner. The CFM uses commercially available microelectromechanical system (MEMS)-based capacitive force sensors with a resolution of 5 nm and a wide force range from 5 nN to 10 mN (Felekis *et al.*, 2011). The modular composition of the CFM provides great flexibility in the choice of microscope optics as well as micropositioners, depending on the needs for scanning range (up to several centimeters), precision of movement, and scanning amplitudes. Recent work showed that CFM is useful for stiffness mapping on both tissues and single cells. Combined with a mechanical model, CFM measurements revealed the mechanical effects of turgor pressure on the apparent stiffness of onion epidermal cells (Routier-Kierzkowska *et al.*, 2012).

To compare and contrast the CFM approach with existing methods, we measured the stiffness of lily (*Lilium longiflorum*) pollen tubes. Previously published work allows for a direct comparison of our results with data produced with the micro-indentation technique. The CFM delivers apparent stiffness values that are in agreement with published data, showing that the pollen tube apex is apparently softer than the shank (Geitmann and Parre, 2004; Zerzour *et al.*, 2009). Our interpretation of the data, however, is different. Using a modelling approach, we show that the difference in the apparent stiffness between the apex and the shank is not necessarily a result of different mechanical properties of the cell wall in these regions, but can be explained exclusively by the geometry of the pollen tube. Thus, although the biochemical composition of the cell wall differs between the tip and the shank, the apparent stiffness after correcting for geometry is similar. Our mechanical model of the pollen tube, based on the finite element method (FEM), allows us to estimate turgor pressure and the Young's modulus of growing lily pollen tubes by combining measurements of the apparent stiffness with changes in geometry that result from osmotic treatments.

RESULTS

Features of the cellular force microscope

For the automated micro-mechanical characterization of living and growing pollen tubes, we developed a versatile system capable of characterizing living cells and organisms of highly diverse and changing morphology under different physiological conditions *in vivo*. By automating the measuring procedure, we were able to conduct multiple, high-resolution stiffness measurements over multiple samples in a small time interval on growing lily pollen tubes.

To achieve this goal, we designed and developed the experimental set-up shown in Figure 1. The system consists of a commercially available MEMS-based force sensor attached to a three-axis positioning system with a scanning range of 27 mm and a resolution of 5 nm along each axis (boxed area in Figure 1a, b) that was mounted on a custom-made stage on an optical, inverted microscope. Further components are a data acquisition system (DAQ card) and a position control unit (Figure 1a). For the control of automated tasks and data logging we designed a custom application in LABVIEW.

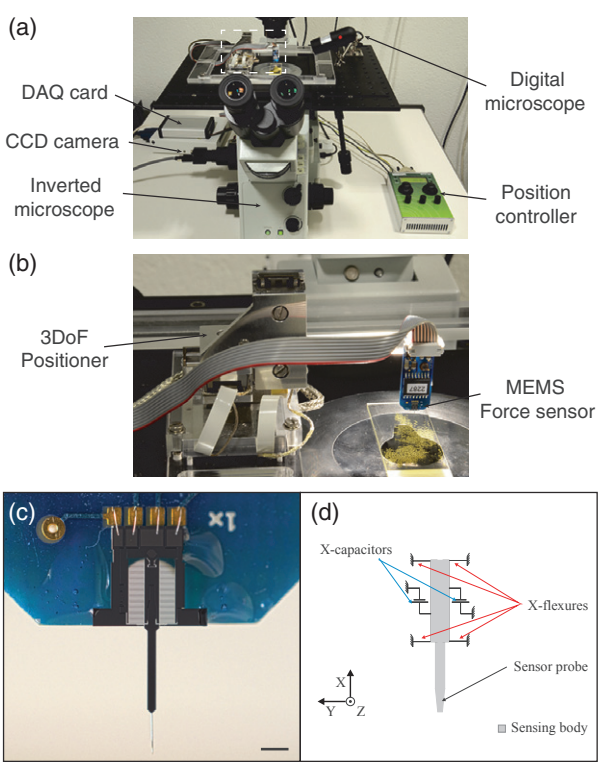

Figure 1. The cellular force microscope (CFM) system.
(a) Overview of the CFM system showing the inverted microscope with a CCD camera and a digital microscope for microelectromechanical system (MEMS) sensor positioning enhancement, the data acquisition (DAQ) card, and the position controller to operate the three-degrees-of-freedom (3DoF) micropositioner (boxed area).
(b) Magnification of the boxed area in (a), showing the 3DoF micropositioner equipped with a MEMS force sensor.
(c) Photograph of the MEMS sensor with a mounted 400–nm radius probe tip (scale bar: 1 mm). (d) Schematic principle of a single-axis MEMS-based capacitance microforce sensor, without the attached tip.

The choice of the probe diameter depends on the properties to be characterized. In this work local elastic properties at the subcellular level were of interest, thus a sharp probe of 2 mm in length with a radius of 0.4 μm was attached to the MEMS-based force sensor, which allows measurements below the mN range (Figure 1c). The sensor probe is positioned vertically above the glass slide holding the lily pollen tubes to be measured. Figure 1d shows a schematic representation of the MEMS-based force sensor.

Apparent stiffness measurements on living pollen tubes

In order to measure the apparent stiffness of turgid, growing lily pollen tubes we germinated pollen on glass slides. Good attachment of the tubes to the slide surface is crucial. Therefore, we tested several slide coatings and found that silane works best. After the initial manual positioning of the sensor probe at the tip of the pollen tube, software-controlled measurements were taken every 5 μm along the tube axis.

As the pollen tubes continued to grow during the experiment, we had to correct for the distance from the tip by taking into account an average growth rate of 135 nm sec^{-1} (±21 nm sec^{-1}, $n = 7$), multiplied with the average time interval between two measurement points of 12.4 sec (±0.9 sec, $n = 6$). From this we calculated a relative movement of the sensor probe away from the tip of 6.7 ± 0.3 μm per interval. We found a sharp increase in the apparent stiffness from 2.7 to 3.8 N m^{-1} over the first 20 μm, after which a plateau was reached (Figure 2). This compares fairly well with previous micro-indentation experiments, which reported an increase in apparent stiffness from 1.3 N m^{-1} at the tip to 1.9 N m^{-1} at 50 μm

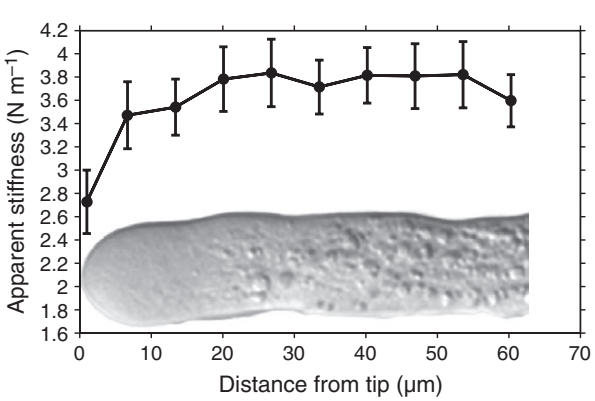

Figure 2. Apparent cell wall stiffness of turgid lily pollen tubes.
Cellular stiffness in the tip region of lily pollen tubes. The curve represents the apparent stiffness of the turgid pollen tube (data are represented as means ± SEMs, $n = 18$). To illustrate the experiment, the apical 60 μm of a lily pollen tube are shown below the curve.

behind the tip for lily (Zerzour *et al.*, 2009) and a similar increase over the first 20 μm for poppy (*Papaver rhoeas*) pollen tubes (Geitmann and Parre, 2004). Pollen from different anthers showed considerable variability in the apparent stiffness of the tubes, ranging from 1.8 to 4.5 N m^{-1} in the plateau phase. As multiple measurements on the same pollen tube were highly consistent, this variation is very likely to be of a biological rather than a technical nature.

In order to determine the contribution of turgor pressure to the measured stiffness, we released the pressure from the pollen tubes by replacing the growth medium with 15% mannitol to induce plasmolysis. To ensure comparability, we used pollen from the same anther and germination experiment for the measurements on turgid and plasmolysed pollen tubes, respectively. After decompression, we found a reduction of the apparent stiffness to values below 1 N m^{-1}, and pollen tubes often collapsed upon contact with the sensor probe, making it difficult to interpret the data. Therefore, in CFM measurements with an indentation depth of 300–400 nm and a probe tip diameter of 800 nm, the difference between turgid and plasmolysed samples implies that turgor pressure makes a large contribution to the apparent stiffness of growing tubes, and therefore must be considered as an important parameter for the estimation of the elastic properties of the pollen tube cell wall. This is in contrast to AFM measurements with an indentation depth of less than 100 nm and a probe tip diameter of 80 nm, where the stiffness measurements are more local and are not influenced by turgor pressure (Milani *et al.*, 2011).

Determination of geometrical parameters

As the cell wall is under tension induced by turgor pressure, the release of turgor leads to shrinkage in the pollen tube. The magnitude of shrinkage can be used to characterize the elastic properties of the cell wall material. To quantify shrinkage after decompression we induced plasmolysis, and determined the change in both the length and the diameter along the pollen tube axis.

Measurements were taken at different distances from the tip over 200 μm, resulting in a mean diameter of 16.0 μm (±0.7 μm, $n = 10$). After plasmolysis, we found a reduction in the mean diameter to 13.4 μm (±0.7 μm, $n = 10$), which corresponds to a shrinkage in the tube diameter of 16.1% (±2.4%, $n = 10$; Figure 3a). In the longitudinal direction, the average shrinkage was 7.5% (±1.95%, $n = 10$), resulting in a ratio between circumferential and longitudinal shrinkage approximating 2:1. For cylindrical cells, the tensional stress in the surface plane of the cell wall is predicted to be twice as high in the circumferential as in the longitudinal direction (Schopfer, 2006). Thus, our data are consistent with a low degree of anisotropy in the wall material, which is expected for pollen tubes without an ordered arrangement of cellulose microfibrils (Anderson *et al.*, 2002; Aouar *et al.*, 2010).

Another important parameter is cell wall thickness. The thinner the cell wall, the stiffer it needs to be to withstand a given tensional stress (Wang *et al.*, 2004). Transmission electron microscopy (TEM) images suggested a wall thickness of 200–300 nm in the tip region of lily pollen tubes. Although the pollen tubes were rapidly frozen and cryo-substituted, providing excellent preservation of the material, it cannot be completely excluded that these relatively thin walls are the result of shrinkage because of sample preparation, as they were dehydrated for TEM (Lancelle and Hepler, 1992; Lancelle *et al.*, 1997). In the model we used 200 nm based on TEM as the lower limit for the wall thickness parameter. To define an upper limit and compare the influence of wall thickness on the Young's modulus, we used confocal laser scanning microscopy (CLSM). Growing pollen tubes were stained with propidium iodide (PI), a fluorescent dye that stains pectins in the cell wall

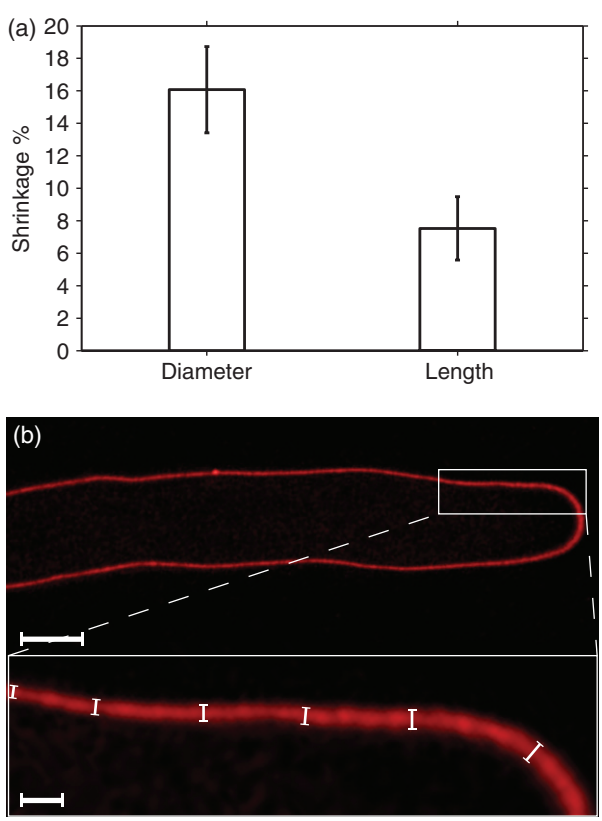

Figure 3. Analysis of osmotic shrinkage and cell wall thickness.
(a) Relative shrinkage of lily pollen tubes after osmotic treatment. Pollen tube diameter and length from the tip to the pollen grain were measured before and after plasmolysis, respectively (data are represented as means ± SEMs, $n = 10$).
(b) Confocal section of a propidium iodide-stained lily pollen tube subjected to deconvolution to measure cell wall thickness (scale bar:10 μm). Multiple measurements were taken in the apical 50 μm of five pollen tubes (data are represented as means ± SEMs). The inlay shows a magnification of the boxed area, with measurements in the tip region (scale bar:2 μm).

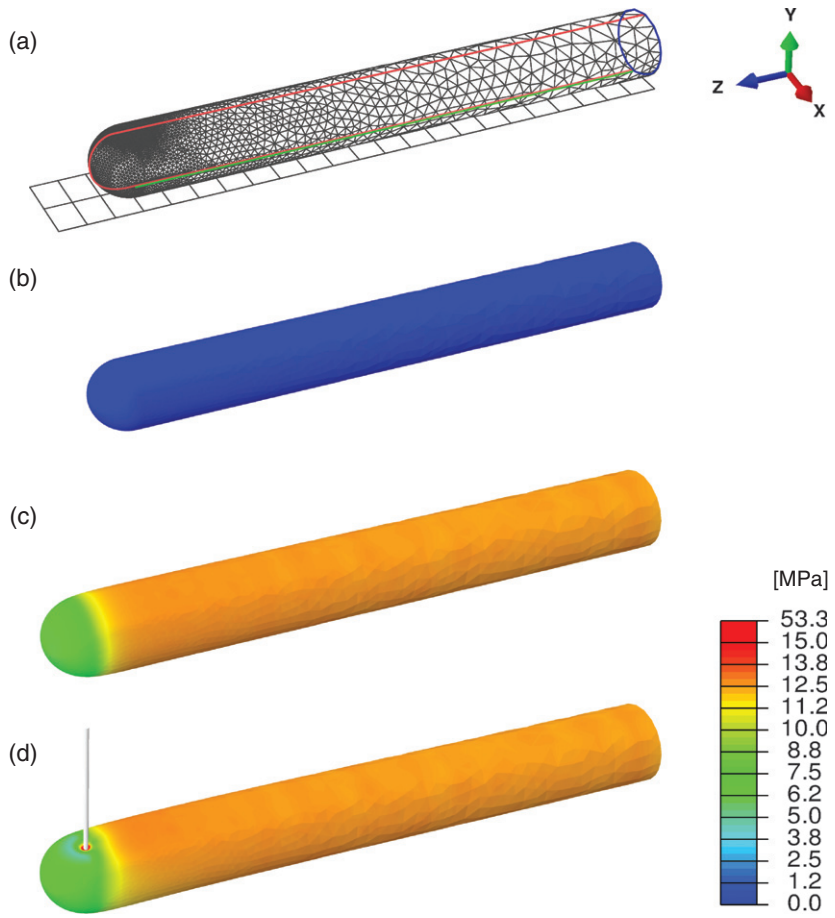

Figure 4. Finite element method (FEM)-based model of the pollen tube.
(a) Boundary conditions and mesh resolution of the FEM simulation. Boundary conditions were applied during the 'inflation' and 'indentation' step. Nodes on the red line were prevented from moving in the *x*–direction during both steps. Nodes on the green line were prevented from moving in the *y*–direction during both steps, and in the *z*–direction only during the 'indentation' step. Nodes on the blue line could not move in the *z*–direction during both steps. The mesh was iteratively refined to provide higher accuracy near the contact patch.
(b, c, d) Stress distribution at three stages of the simulation. The stress-free reference configuration (b) was first pressurized (c). Note the differences in maximum principal stress between the apex and the cylindrical part. In a second step, the pressurized structure was indented by a rigid probe in the *y*–direction. This resulted in a local stress concentration (d) Color coding shows the maximal principal stress in MPa.

without affecting cytoplasmic streaming, and thus pollen viability (Tian *et al.*, 2006). Confocal sections of PI-stained tubes were deconvolved and measurements were taken at different positions of the cell wall within the apical 50 μm, giving an average value of 699 nm (±65 nm, $n = 5$; Figure 3b). Taking into account that this is probably an overestimation because of light scattering, but that on the other hand we ignore the contribution of cellulose and callose to cell wall thickness, we used 700 nm based on CLSM as the upper limit for the wall thickness parameter in a FEM-based model of the pollen tube.

Finite element method-based model of the pollen tube

Apparent stiffness measurements reflect a combination of mechanical and geometrical properties. In order to separate the various influences on stiffness, it is essential to fit the data with a mechanical model that captures all of the relevant aspects. In the following section we present a quasi-static continuum mechanics model of a pollen tube, in which we reproduce our osmotic and CFM measurements. The model is subdivided into two steps. The first step describes the inflation of a pollen tube section as a result of osmotic water uptake. The second step simulates the contact of the inflated structure during indentation with a rigid probe, i.e. the MEMS-based force sensor.

The initial geometry of the pollen tube is represented by a cylindrical shell, which is attached to a hemispherical shell with radius and thickness based on microscopical data. The length of the section is chosen to be large enough to minimize the influence of boundary conditions, which are applied to the distal circular edge (Figure 4a).

Cellulose is thought to be the main load-bearing constituent in the cell wall. If it is deposited in an oriented manner, the cell wall is likely to show mechanical anisotropy

(Erickson, 1976; Fry, 1995; Geitmann and Steer, 2006; Schopfer, 2006). Although our shrinkage experiment suggests rather isotropic properties of the pollen tube cell wall, we cannot exclude a certain degree of anisotropy. To allow for this possibility, we assigned the shell with an orthotropic, linear elastic material model. This constitutive model is able to capture different elastic behaviours in longitudinal and circumferential directions, respectively. It is fully characterized by the compliance matrix, which relates stresses and strains (see Appendix S1), and three material directions that describe the structural anisotropy in each point. The parameters within the compliance matrix are called engineering constants. Three Young's moduli describe elasticity in each direction when the material is subject to loading in that same direction. Six Poisson's ratios, of which three are independent, describe how much the material stretches in one direction because of loading in a different direction (Poisson effect). Finally, three shear moduli describe shear flexibility.

As we were not able to fit nine independent parameters, we made several assumptions on the mechanics of the cell wall. In particular we assumed that: (i) the material is fully compressible (i.e. all Poisson's ratios are zero); (ii) that the Young's modulus in the direction normal to the surface is the same as in the longitudinal direction; and (iii) all shear moduli equal $E_l/2$, where E_l denotes the longitudinal Young's modulus.

Assumption (i) implies that strain in any direction depends only on the stress in that direction, and the effects of non-zero Poisson's ratios are discussed in Appendix S1. Assumption (ii) allows for anisotropy in the longitudinal versus the circumferential direction. Finally, the choice of the shear moduli in assumption (iii) equals the one that we would expect for a fully compressible, isotropic material of stiffness E_l. This assumption is of low importance as shear stresses were significantly lower than principle stresses in all simulations.

The model includes two quasi-static steps. In a first step, the virtual pollen tube (Figure 4b) is inflated by a uniform pressure, which acts on the inside of the cell wall. As a result, the shell extends in both circumferential and longitudinal directions (Figure 4c). The exact level depends on the dimensions of the shell, the level of turgor pressure and the material coefficients. As we chose the material to be fully compressible, extension in the longitudinal and the circumferential directions are independent. Although the geometry of the pollen tube is not perfectly cylindrical, the global deformation obeys Laplace's law of stress distribution in a cylindrical pressure vessel quite closely. If this formula is combined with the linear elastic material law of Abaqus (i.e. with logarithmic strain), it reads:

$$\frac{Pr}{d} = \sigma_c = E_c \cdot \log(\lambda_c); \quad \frac{Pr}{2d} = \sigma_l = E_l \cdot \log(\lambda_l)$$

where P is the turgor pressure, r is the radius and d is the thickness of the cylinder, σ_c and σ_l are Cauchy stresses, E_c and E_l are Young's moduli, and λ_c and λ_l are the initial stretch ratios in circumferential and longitudinal directions, respectively. It should be noted that the initial stretch ratios only depend on the dimensionless quantity pressure over Young's modulus. This means that a certain stretch ratio can be reached by either having soft material and little pressure or stiff material and high pressure.

In the second step of the simulation, the pressurized shell is indented with a rigid probe, which has the shape of a hemisphere that is connected to a cylinder. The scanning mode of CFM is simulated by placing the probe at varying distances from the tip and by moving it vertically in small steps. Once the probe touches the pollen tube, a frictionless contact between the pollen tube and the probe (the supporting plane) is simulated (Figure 4d). Depending on the surface geometry, the force exerted onto the probe by the pollen tube might not be aligned with the axis of indentation. As the CFM sensor is designed to only measure forces in the direction of indentation, the vertical component is used for stiffness computations. The apparent stiffness is then calculated as the change in force over the change in vertical displacement. During both steps of the simulation, the same set of boundary conditions described in Figure 4a are applied.

Simulation using a finite element method-based model reveals turgor pressure and the Young's modulus of pollen tubes

To test our model we used the parameters summarized in Table 1. A point 40 μm behind the tip was fitted with the apparent stiffness data we measured before (Figure 2, see Appendix S1 for details). The simulation revealed an apparent stiffness pattern very similar to what we found in

Table 1 Model parameters

Pollen tube parameters					Indenter parameters		Experimental parameters	
r_{ref} (μm)	l_{ref} (μm)	λ_c	λ_l	Wall thickness (nm)	r_{ind} (μm)	Indenter shape	Target force (μN)	Target stiffness (N m^{-1})
6.7	100	1.161	1.075	200 700	0.4	round	3.5	3.7

r_{ref}, reference radius; l_{ref}, length of reference modeling section; λ_c, circumferential stretch ratio; λ_l, longitudinal stretch ratio; r_{ind}, indenter radius.

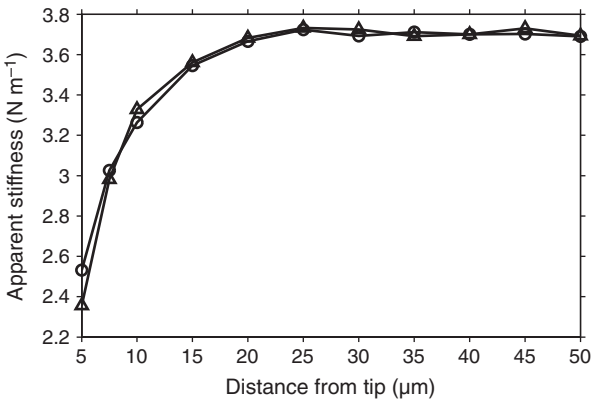

Figure 5. Indentation simulation reveals the quality of the finite element method-based model.
Indentation simulation with different cell wall thicknesses: the model was fitted with apparent stiffness data 40 μm behind the tip using the parameters shown in Table 1. The simulated apparent stiffness values along the entire length of 50 μm from the pollen tube tip are very similar to those obtained from actual measurements (Figure 2). Cell wall thickness has a negligible influence on the apparent stiffness. △, 200-nm-thick cell wall; ○, 700–nm-thick cell wall.

our measurements (compare Figures 5 and 2). Moreover, we did not find any notable differences in the apparent stiffness between model fits performed with a cell wall thickness of 200 and 700 nm, respectively.

When we assumed a 200–nm-thick wall, turgor pressure was 0.33 MPa, slightly higher than the 0.30 MPa determined for a 700–nm-thick wall (Table 2). Indeed, a turgor pressure of around 0.3 MPa is in agreement with values measured with a pressure probe, but significantly different from 0.8 MPa calculated by the incipient plasmolysis method (Benkert *et al.*, 1997).

In addition to turgor pressure, our model reveals that the Young's modulus in the longitudinal (E_l) and the circumferential (E_c) direction are almost equal, reflecting our finding that circumferential and longitudinal shrinkage induced by plasmolysis occurred with a ratio of 2:1. As expected, we found considerably different Young's moduli for 200- and 700–nm-thick cell walls, with about 90 and 20 MPa, respectively. Both values, however, lie in the range of rubber, indicating that the cell wall of pollen tubes is very elastic.

Table 2 Turgor pressure and Young's modulus depend on cell wall thickness

	Cell wall thickness	
	200 (nm)	700 (nm)
P (MPa)	0.33	0.30
E_l (MPa)	89.31	22.77
E_c (MPa)	86.53	22.06

P, turgor pressure; E_l, Young's modulus in the longitudinal direction; E_c, Young's modulus in the circumferential direction.

DISCUSSION

Stiffness gradient along the pollen tube axis can be explained by geometry

The expansion of pollen tubes takes place exclusively at the tip, indicating that this region may be softer than the shank. In agreement with this, it has been proposed that new wall material is deposited near the pollen tube tip (Holdaway-Clarke and Hepler, 2003; Chebli and Geitmann, 2007; Zonia and Munnik, 2008). Evidence for the hypothesis of a softer tip came from observations showing that pectins are strongly methyl-esterified at the tip and become cross-linked by Ca^{2+} in more distal parts (Li *et al.*, 1994). Crystalline cellulose, as well as callose, is absent from the apical region of the pollen tube (Aouar *et al.*, 2010; Geitmann, 2010). FEM-based modeling provided further evidence that a gradient of extensibility along the pollen tube would explain growth localized to the tip (Fayant *et al.*, 2010).

The apparent stiffness pattern we found along the apical region resembles previous results, showing that the tip appears softer than the more distal regions of the shank. This has been interpreted as an indication that the mechanical properties of the cell wall must be different at the tip, in agreement with expansion taking place exclusively at the tip of growing pollen tubes (Geitmann and Parre, 2004; Zerzour *et al.*, 2009). However, our results indicate that, assuming uniform mechanical cell wall properties for the entire pollen tube, the reduction in apparent stiffness at the tip can be explained solely by the geometry of the pollen tube. As we measure in the vertical direction we have a gradually increasing angle of tilt between the direction of indentation and the surface towards the apex. This means that even if the forces were the same in magnitude, we would expect microindentation methods to report lower values on the hemispherical part of the apex, because forces are measured only in the direction of probe indentation. Geometry can also cause a gradient in stiffness near the apex in the cylindrical portion of the tube, caused by turgor-induced pre-tension of the cell wall. In the cylindrical part, there is twice as much maximum principal tension as in the hemispherical apex. As a result of this difference, the cylindrical part acts like a guitar-string under high tension, which is harder to deflect than the same string under lower tension. This effect would also explain the qualitative difference between the prediction of our model and the one from Bolduc and colleagues (Bolduc *et al.*, 2006). Albeit they also constructed an FEM-based model of the pollen tube, they did not include turgor pressure, and thus did not observe the pre-tension effect. As a result, their model predicted the apex to appear stiffer than the shank, based on geometry alone.

Although there are well-documented gradients in the biochemical composition of the cell wall between the tip

and the shank (Mascarenhas, 1975; Heslop-Harrison, 1987; Ferguson *et al.*, 1998; Fayant *et al.*, 2010; Derksen *et al.*, 2011), our experimental data fit with a homogeneous material. This is probably because the effects of geometry and pressure mask the elastic differences within the cell wall. To measure these differences it would be necessary to indent normal to the surface, which is not possible with the MEMS-based force sensors available, and to reduce turgor pressure. Fayant and colleagues propose a model of pollen tube growth where extensibility is much higher in the tip than in the shank, but it is unclear how extensibility relates to elasticity. Firstly, in our model we have assumed that the cell wall is fully compressible; however, no data are available concerning the Poisson's ratio of pollen tube cell walls. The effect of a change of the Poisson's ratio between 0 (fully compressible) and 0.5 (low compressibility) could change the Young's moduli up to twofold (Table S1). Secondly, we are aware that the assumption of frictionless contact between the pollen tube and the CFM probe is arbitrary, but that it may play a role at the apex as we observed that slippage can occur if we do not indent perpendicularly. This issue could be solved by adding rotational degrees of freedom to the micropositioner, which, on the other hand, would make the manual and automatic control of such a system a very demanding task. Another solution for this problem would be to use two-dimensional force sensors that are capable of measuring forces in the vertical as well as in the horizontal direction at the same time. However, multi-axial force sensors are not currently commercially available for the force range and resolution we need.

CFM is particularly well suited to assess cellular stiffness

Compared with other microindentation methods, the CFM offers higher resolution and an increased level of automation and control of the experimental parameters. Although AFM offers higher resolution, it has smaller positioning and force ranges. The possibility to attach thin and long probes to the MEMS sensors allows the measurement of cells or tissue regions that are difficult to access by other methods. In addition, different mechanical properties of cells or tissues can be investigated by choosing a suitable probe shape and diameter.

The CFM has proven to be a versatile system to measure forces on living pollen tubes with high resolution, showing that this device can be used on fast-growing cells with a very low apparent stiffness compared with previous applications (Routier-Kierzkowska *et al.*, 2012). The wide force range that is covered by the possibility to mount different types of sensors makes it also suitable for animal cells and tissues. Indeed, the same type of sensor has been used previously to measure the mechanical properties of mouse oocytes before and after fertilization (Sun and Nelson, 2007). In combination with fluorescence microscopy it may be possible to monitor intracellular responses to locally applied mechanical stress. The large scanning area makes it possible to get stiffness maps of entire organs, and thus shed some light onto the interplay between mechanical and molecular effects during growth and development at an unprecedented resolution.

A soft shell with a hard core

The FEM-based modelling combined with our experiments revealed a Young's modulus of the pollen tube cell wall that approximately corresponds to rubber, equal to 20 and 90 MPa for a cell wall thickness of 200 and 700 nm, respectively. To our knowledge, there is no reference value for the elasticity of pollen tube cell walls available, and generally values for individual plant cells are sparse.

Wang and colleagues estimated the wall elasticity of suspension culture cells derived from root radicle calli of tomato to a value between 1.4 and 4.2 GPa, which depends on the chosen model assumptions, such as cell wall thickness, initial stretch ratio or the magnitude of cell deformation, as well as on experimental parameters like the pH value of the cultivation medium (Wang *et al.*, 2004, 2008). A possible explanation for the remarkable difference in cell wall stiffness between cultured tomato cells and lily pollen tubes with a Young's modulus of 20–90 MPa could be the lower content of cellulose in the pollen tubes. It has been reported that pollen tube cell walls contain 2–10% cellulose, rather than the 20–30% found in other types of plant cells (Steer and Steer, 1989; Schlupmann *et al.*, 1994).

Pollen tubes are fast-growing cells. In plants with a solid style, such as Arabidopsis, they first have to penetrate the stigmatic tissue and the transmitting tract before reaching the ovules. Lily, on the other hand, has a hollow style where the pollen tubes grow on the surface of the transmitting tissue, between the epidermal cells and the cuticle (Lord, 2000). Attraction by the ovule forces the tubes to make sudden changes in direction and, in the process of fertilization, the pollen tubes need to push through the micropylar opening before penetrating a synergid cell. Meeting these requirements may be easier for a relatively stiff cell with a flexible cell wall.

Our engineering-style FEM-based mechanical model allows us to analyze the mechanical behavior of a pressurized pollen tube. By measuring the apparent stiffness, cell wall thickness and the initial stretch ratio, we were able to calculate turgor pressure as well as the elasticity of the cell wall. This opens the door for further studies on cell wall mutants to investigate the influence of an altered cell wall composition on the mechanical properties of the pollen tube wall. It will be possible to correlate these data with growth rate, resistance to bursting and fertilization success. Furthermore, it will be interesting to make use of genetic or molecular sensors to shed light on the effects of locally applied mechanical stresses on intracellular

processes, such as calcium fluxes, the production of reactive oxygen species or cytoskeleton dynamics, all of which play an important role in pollen tube growth.

EXPERIMENTAL PROCEDURES

Pollen tube growth

Anthers of lily (*Lilium longiflorum*) were frozen at −80°C until used. Frozen pollen was brushed on silane-coated slides (Science Services GmbH, http://scienceservices.de), incubated for 30 min in a moisture chamber, subsequently covered with growth medium [10% sucrose, 5 mM 2–(*N*–morpholino) ethanesulfonic acid (MES), 5 mM KNO_3, 0.13 mM $Ca(NO_3)_2$, 0.16 mM H_3BO_3], and incubated at 22°C for 1.5–2.0 h. The slides were washed three times with growth medium to get rid of non-sticking pollen tubes, and the remaining tubes were covered with growth medium for stiffness measurements. The growth rate was measured from images taken at a 5–min time intervals (two repetitions per pollen tube). For the induction of plasmolysis the growth medium was replaced with 15% mannitol.

MEMS equipment

A commercially available single-axis capacitive MEMS-based microforce-sensing probe (FT–S540; FemtoTools GmbH, http://femtotools.com) was used for our experiments. Each sensor is individually pre-calibrated by the manufacturer following an SI-traceable calibration procedure that ensures the precision of the measurement system.

The working principle of the sensor is schematically shown in Figure 1d. The sensor consists of a movable body with an attached probe suspended by four flexures within an outer frame. A force applied to the probe in the *x*–direction results in a relative motion of the body and the outer frame, which can be measured as a change in the capacitance of the attached capacitive electrodes. Two capacitive changes with opposite signs are differentially measured using a capacitance-to-voltage converter (MS3110; Irvine Sensors Inc., http://www.irvine-sensors.com), resulting in a linear output.

As a result of the symmetric design of this sensor, with its four flexures, parallel motion of the movable body as it is deflected can be achieved, making this design superior to most cantilever-type sensors. Furthermore, because of its long sensing probe, the sensor can access three-dimensional structures, even in depressions, making the system suitable for measurements of organisms and tissues with diverse and changing morphology.

Software and data acquisition

For the integration of the components comprising the CFM system presented in the system description above, we used a custom application developed in LABVIEW (National Instruments, http://www.ni.com). The application performs the control of the automated tasks as well as the data logging. In addition, a user interface (UI) for the control of the experimental parameters was developed. The data acquisition is performed using a National Instruments USB-6009 DAQ Card (National Instruments, http://www.ni.com). The sampling rate used is 100 Hz for the coarse approach phase, and 50 Hz for the fine approach and the scanning mode. These values were chosen such that the desired force resolution, which is based on the noise signal, was achieved. The MEMS sensor is supplied with 5 V and the sensor's analog signal is acquired too. The data collected are the absolute *X*, *Y* and *Z* position of the microrobot, the sensor's analog signal (voltage), the calculated force sensed at the tip, the timestamp for each of the aforementioned values, and the type of movement performed at that timestamp, i.e. fine or coarse approach and scanning mode. All these data are logged for post-processing.

In addition to acquisition and logging the software provides control over the automated measuring procedure. We use two different types of control methods. The first method is position feedback, when we move from one measurement location to the next, when we position the end effector at a specific distance from the cell surface, and also when we perform the unloading phase. The second method is the control of the movement based on force feedback. This method is used in the actual measurement phase, and comprises the coarse approach, the fine approach, and the loading phase.

All the experimental parameters, such as contact and measurement force, step speed and size, scanning speed and amplitude, distance from the cell surface at starting position and scanning mesh properties are defined at the beginning of the experiment.

Stiffness measurements

Lily pollen tubes adhered to silane-coated slides (Science Services, http://www.scienceservices.de) were focused at a 400 × magnification with differential interference contrast (DIC) optics on an inverted microscope (IX 71; Olympus, http://www.olympus-global.com). After the sensor tip was positioned manually on the pollen tube at the starting point of the measurement series, control was transferred to LABVIEW. At each point we took four measurements with four scans (see below), from each of which we calculated the mean stiffness values.

Every individual measurement started with a 'coarse approach' using the step mode of the actuator to identify the surface of the pollen tube. Then the sensor retracted from the sample by a previously defined distance before it started the 'fine approach' to indent the tube until a threshold force (F_{max}) of 4 μN was reached. The differences between the coarse and the fine approaches are the step amplitude and frequency. Larger values for both parameters ensure faster movement, and thus we use this approach to speed up the contact detection between the tip and the sample. At this point the movement switched to the scan mode and performed a number of loading and unloading cycles. The reason for using this positioning method for the measurements is that with the scan mode a smoother and continuous movement is achieved. As the loading and unloading cycles take place past the contact point, adhesion effects are avoided.

Data analysis was performed with MATLAB (MathWorks, http://www.mathworks.ch). First, the contact point between the sensor probe tip and the pollen tube surface was estimated from the force–displacement curve acquired during the fine approach. Starting from the deepest point of indentation, the algorithm finds the first point for which the stiffness is below a predefined threshold. For indenting in liquid medium, the surface tension results in a positive force measured by the sensor before entering into contact with the sample. As a consequence, the force at the maximal indentation depth can differ from the user-defined maximal force threshold. Hence, we corrected the measured force such that the load at the contact point is set to zero. Quantification of the surface tension effect revealed a stiffness of the liquid medium of about 0.02 Nm^{-1}, which is two orders of magnitude lower than the apparent stiffness of the pollen tubes, and can therefore be neglected.

Stiffness values were determined from the slope of the force–displacement curves acquired during scan mode by performing a least-squares linear fit separately for each phase of the oscillations, as described previously (Routier-Kierzkowska *et al.*, 2012).

Estimation of geometrical parameters

To measure the shrinkage of the pollen tubes, we took DIC images before and after plasmolysis. The diameter and the length of the pollen tubes were measured with ImageJ (http://rsbweb.nih.gov/ij).

For the estimation of cell wall thickness we stained actively growing pollen tubes with growth medium containing 30 μM propidium iodide. After incubation for 3–5 min the staining solution was replaced with growth medium. Using a confocal laser scanning microscope (Leica SP2, http://www.leica-microsystems.com), we made longitudinal optical sections with a thickness of 120 nm through the pollen tube. The image stacks where then deconvolved with 3D HUYGENS deconvolution software (Scientific Volume Imaging, http://www.svi.nl). The stack slice showing the pollen tube section with the largest diameter was chosen to measure the thickness of the cell wall using ImageJ.

FEM implementation

The mechanical model was implemented in ABAQUS/STANDARD (Simulia, http://www.3ds.com) and solved based on finite deformation theory. For the representation of the pollen tube we chose linear triangular shell elements (S3). The discretization was individually computed for each indentation position, based on an iterative mesh refinement procedure. The contact problems between pollen tube and indenter, and between pollen tube and support, were solved by the node-to-node, augmented Lagrange algorithm.

Given our set of assumptions, there are three model parameters that cannot be measured directly. These are the turgor pressure and the longitudinal and circumferential Young's moduli. In order to obtain quantitative estimates for those parameters, we fitted our model to the experimental data. The quality of fit was assessed based on two criteria. First, the model should show the same level of stretch in longitudinal and circumferential direction as measured during the osmotic assays. Second, it should have the same apparent stiffness when indented 40 μm behind the apex.

ACKNOWLEDGEMENTS

We thank Simon Muntwyler and Felix Beyeler (FemtoTools, Buchs, Switzerland) for technical advice on the sensors, Daniel Bollier (University of Zürich) for workshop support, and anonymous reviewers for helpful comments. This work was supported by the University of Zürich, the University of Bern, and the Research and Technology Development Project 'Plant Growth in a Changing Environment', supported by SystemsX.ch, the Swiss Initiative in Systems Biology (to CR, BJN, RSS and UG).

SUPPORTING INFORMATION

Additional Supporting Information may be found in the online version of this article.

Table S1. Estimated pressure and elasticity for Poisson's ratio varying 'in plane'.

Appendix S1. We describe the influence of the chosen Poisson's ratio on the Young's moduli and turgor pressure resulting from our simulated experiment, and present the mathematical background.

REFERENCES

Anderson, J.R., Barnes, W.S. and Bedinger, P. (2002) 2,6-Dichlorobenzonitrile, a cellulose biosynthesis inhibitor, affects morphology and structural integrity of petunia and lily pollen tubes. *J. Plant Physiol.* **159**, 61–67.

Aouar, L., Chebli, Y. and Geitmann, A. (2010) Morphogenesis of complex plant cell shapes: the mechanical role of crystalline cellulose in growing pollen tubes. *Sex. Plant Reprod.* **23**, 15–27.

Benkert, R., Obermeyer, G. and Bentrup, F.W. (1997) The turgor pressure of growing lily pollen tubes. *Protoplasma* **198**, 1–8.

Bolduc, J.F., Lewis, L.J., Aubin, C.E. and Geitmann, A. (2006) Finite-element analysis of geometrical factors in micro-indentation of pollen tubes. *Biomech. Model. Mechan.* **5**, 227–236.

Burton, R.A., Gidley, M.J. and Fincher, G.B. (2010) Heterogeneity in the chemistry, structure and function of plant cell walls. *Nat. Chem. Biol.* **6**, 724–732.

Chanliaud, E. and Gidley, M.J. (1999) *In vitro* synthesis and properties of pectin/*Acetobacter xylinus* cellulose composites. *Plant J.* **20**, 25–35.

Chebli, Y. and Geitmann, A. (2007) Mechanical principles governing pollen tube growth. *Funct. Plant Sci. Biotechnol.* **1**, 232–245.

Cosgrove, D.J. (1993) Wall extensibility: its nature, measurement and relationship to plant cell growth. *New Phytol.* **124**, 1–23.

Cosgrove, D.J. (2005) Growth of the plant cell wall. *Nat. Rev. Mol. Cell Biol.* **6**, 850–861.

Derksen, J., Janssen, G.J., Wolters-Arts, M., Lichtscheidl, I., Adlassnig, W., Ovecka, M., Doris, F. and Steer, M. (2011) Wall architecture with high porosity is established at the tip and maintained in growing pollen tubes of *Nicotiana tabacum*. *Plant J.* **68**, 495–506.

Edge, S., Steele, D.F., Chen, A., Tobyn, M.J. and Staniforth, J.N. (2000) The mechanical properties of compacts of microcrystalline cellulose and silicified microcrystalline cellulose. *Int. J. Pharm.* **200**, 67–72.

Erickson, R.O. (1976) Modeling of plant growth. *Annu. Rev. Plant Physiol.* **27**, 407–434.

Fayant, P., Girlanda, O., Chebli, Y., Aubin, C., Villemure, I. and Geitmann, A. (2010) Finite element model of polar growth in pollen tubes. *Plant Cell* **22**, 2579–2593.

Felekis, D., Muntwyler, S., Vogler, H., Beyeler, F., Grossniklaus, U. and Nelson, B.J. (2011) Quantifying growth mechanics of living, growing plant cells *in situ* using microrobotics. *Micro. Nano. Lett.* **6**, 311–316.

Ferguson, C., Teeri, T.T., Siika-aho, M., Read, S.M. and Bacic, A. (1998) Location of cellulose and callose in pollen tubes and grains of *Nicotiana tabacum*. *Planta* **206**, 452–460.

Fernandez-Sanchez, M.E., Serman, F., Ahmadi, P. and Farge, E. (2010) Mechanical induction in embryonic development and tumor growth integrative cues through molecular to multicellular interplay and evolutionary perspectives. *Methods Cell Biol.* **98**, 295–321.

Fry, S.C. (1995) Polysaccharide-modifying enzymes in the plant cell wall. *Annu. Rev. Plant Physiol. Plant Mol. Biol.* **46**, 497–520.

Geitmann, A. (2006) Experimental approaches used to quantify physical parameters at cellular and subcellular levels. *Am. J. Bot.* **93**, 1380–1390.

Geitmann, A. (2010) How to shape a cylinder: pollen tube as a model system for the generation of complex cellular geometry. *Sex. Plant Reprod.* **23**, 63–71.

Geitmann, A. and Parre, E. (2004) The local cytomechanical properties of growing pollen tubes correspond to the axial distribution of structural cellular elements. *Sex. Plant Reprod.* **17**, 9–16.

Geitmann, A. and Steer, M. (2006) The architecture and properties of the pollen tube cell wall. In *The Pollen Tube* (Malhó, R., ed.). Berlin/Heidelberg: Springer-Verlag, pp. 177–200.

Hepler, P.K., Kunkel, J.G., Rounds, C.M. and Winship, L.J. (2012) Calcium entry into pollen tubes. *Trends Plant Sci.* **17**, 32–38.

Heslop-Harrison, J. (1987) Pollen germination and pollen-tube growth. *Int. Rev. Cytol.* **107**, 1–78.

Holdaway-Clarke, T.L. and Hepler, P.K. (2003) Control of pollen tube growth: role of ion gradients and fluxes. *New Phytol.* **159**, 539–563.

Kutschera, U. (1996) Cessation of cell elongation in rye coleoptiles is accompanied by a loss of cell-wall plasticity. *J. Exp. Bot.* **47**, 1387–1394.

Lancelle, S.A. and Hepler, P.K. (1992) Ultrastructure of freeze-substituted pollen tubes of *Lilium longiflorum*. *Protoplasma* **167**, 215–230.

Lancelle, S.A., Cresti, M. and Hepler, P.K. (1997) Growth inhibition and recovery in freeze-substituted *Lilium longiflorum* pollen tubes: structural effects of caffeine. *Protoplasma* **196**, 21–33.

Li, Y.Q., Chen, F., Linskens, H.F. and Cresti, M. (1994) Distribution of unesterified and esterified pectins in cell walls of pollen tubes of flowering plants. *Sex. Plant Reprod.* **7**, 145–152.

Lord, E. (2000) Adhesion and cell movement during pollination: cherchez la femme. *Trends Plant Sci.* **5**, 368–373.

Martin, A.C. (2010) Pulsation and stabilization: contractile forces that underlie morphogenesis. *Dev. Biol.* **341**, 114–125.

Mascarenhas, J.P. (1975) The biochemistry of angiosperm pollen development. *Bot. Rev.* **41**, 259–314.

Milani, P., Gholamirad, M., Traas, J., Arneodo, A., Boudaoud, A., Argoul, F. and Hamant, O. (2011) *In vivo* analysis of local wall stiffness at the shoot apical meristem in *Arabidopsis* using atomic force microscopy. *Plant J.* **67**, 1116–1123.

Mirabet, V., Das, P., Boudaoud, A. and Hamant, O. (2011) The role of mechanical forces in plant morphogenesis. *Annu. Rev. Plant Biol.* **62**, 365–385.

Parre, E. and Geitmann, A. (2005) More than a leak sealant. The mechanical properties of callose in pollen tubes. *Plant Physiol.* **137**, 274–286.

Peaucelle, A., Braybrook, S.A., Le Guillou, L., Bron, E., Kuhlemeier, C. and Höfte, H. (2011) Pectin-induced changes in cell wall mechanics underlie organ initiation in *Arabidopsis*. *Curr. Biol.* **21**, 1720–1726.

Pertl, H., Pockl, M., Blaschke, C. and Obermeyer, G. (2010) Osmoregulation in *Lilium* pollen grains occurs via modulation of the plasma membrane H+ ATPase activity by 14-3-3 proteins. *Plant Physiol.* **154**, 1921–1928.

Qin, Y. and Yang, Z. (2011) Rapid tip growth: insights from pollen tubes. *Semin. Cell Dev. Biol.* **22**, 816–824.

Routier-Kierzkowska, A.L., Weber, A., Kochova, P., Felekis, D., Nelson, B.J., Kuhlemeier, C. and Smith, R.S. (2012) Cellular force microscopy for *in vivo* measurements of plant tissue mechanics. *Plant Physiol.* **158**, 1514–1522.

Schlupmann, H., Bacic, A. and Read, S.M. (1994) Uridine diphosphate glucose metabolism and callose synthesis in cultured pollen tubes of *Nicotiana alata* Link et Otto. *Plant Physiol.* **105**, 659–670.

Schopfer, P. (2006) Biomechanics of plant growth. *Am. J. Bot.* **93**, 1415–1425.

Smith, A.E., Moxham, K.E. and Middelberg, A.P.J. (1998) On uniquely determining cell wall material properties with the compression experiment. *Chem. Eng. Sci.* **53**, 3913–3922.

Steer, M.W. and Steer, J.M. (1989) Pollen tube tip growth. *New Phytol.* **111**, 323–358.

Sun, Y. and Nelson, B.J. (2007) MEMS capacitive force sensors for cellular and flight biomechanics. *Biomed. Mater.* **2**, S16–S22.

Tian, G.W., Chen, M.H., Zaltsman, A. and Citovsky, V. (2006) Pollen-specific pectin methylesterase involved in pollen tube growth. *Dev. Biol.* **294**, 83–91.

Tomos, A.D. and Leigh, R.A. (1999) The pressure probe: a versatile tool in plant cell physiology. *Annu. Rev. Plant Physiol. Plant Mol. Biol.* **50**, 447–472.

Wang, C.X., Wang, L. and Thomas, C.R. (2004) Modelling the mechanical properties of single suspension-cultured tomato cells. *Ann. Bot.* **93**, 443–453.

Wang, C.X., Wang, L., McQueen-Mason, S.J., Pritchard, J. and Thomas, C.R. (2008) pH and expansin action on single suspension-cultured tomato (*Lycopersicon esculentum*) cells. *J. Plant. Res.* **121**, 527–534.

Wei, C. and Lintilhac, P.M. (2007) Loss of stability: a new look at the physics of cell wall behavior during plant cell growth. *Plant Physiol.* **145**, 763–772.

Wei, C., Lintilhac, L.S. and Lintilhac, P.M. (2006) Loss of stability, pH, and the anisotropic extensibility of *Chara* cell walls. *Planta* **223**, 1058–1067.

Young, T. (1845) *Course of Lectures on Natural Philosophy and the Mechanical Arts*. London: Taylor and Walton.

Zamir, E.A. and Taber, L.A. (2004) On the effects of residual stress in microindentation tests of soft tissue structures. *J. Biomech. Eng.* **126**, 276–283.

Zerzour, R., Kroeger, J. and Geitmann, A. (2009) Polar growth in pollen tubes is associated with spatially confined dynamic changes in cell mechanical properties. *Dev. Biol.* **334**, 437–446.

Zhao, L., Schaefer, D., Xu, H., Modi, S.J., Lacourse, W.R. and Marten, M.R. (2005) Elastic properties of the cell wall of *Aspergillus nidulans* studied with atomic force microscopy. *Biotechnol. Prog.* **21**, 292–299.

Zonia, L. and Munnik, T. (2008) Vesicle trafficking dynamics and visualization of zones of exocytosis and endocytosis in tobacco pollen tubes. *J. Exp. Bot.* **59**, 861–873.

